LES-CMC SIMULATIONS OF TURBULENT HYDROGEN FLAME IN A VITIATED AIR CO-FLOW

I. Stanković* and B. Merci*

Ivana.Stankovic@UGent.be

*Ghent University - UGent, Department of Flow, Heat and Combustion Mechanics, Belgium

Abstract

This work concerns numerical simulation of hydrogen flames in a vitiated co-flow, using Large Eddy Simulation (LES) and Conditional Moment Closure (CMC) as sub-grid turbulence-chemistry model. A qualitative description of the simulation results, by examining the instantaneous resolved temperature and species mass fraction fields, is provided. The structure of the lifted flame is further investigated by comparing the experimentally measured temperature and species mass fraction profiles to the simulation results. The model captures the axial and radial profiles of mixture fraction, temperature and major species, such as H_2, O_2, N_2, OH and H_2O, provided the co-flow temperature is chosen appropriately. The sensitivity of prediction to boundary conditions is also explored. A lift-off height of ten nozzle diameters was obtained experimentally for a co-flow temperature of 1045K. In the calculations, the best agreement was obtained for the co-flow temperature of 1030K, which is within experimental uncertainty. Finally, the stabilization mechanisms are addressed. No evidence of premixed flame propagation is found: the diffusion in physical space is negligible for all studied conditions. Upstream of the flame base, a clear convection-reaction balance is observed, with the scalar dissipation rate being important as well.

Introduction

The flame under study is a turbulent lifted jet flame of hydrogen, diluted with nitrogen, issuing into a wide co-flow of vitiated air. Lifted flames are a challenging problem since the flame at the flame base is unstable and involves a significant degree of interactions between chemical and flow timescales. However, the simple burner geometry developed by Cabra et al. [1] at Berkeley University, provides a good base for studying complex lifted flames and turbulence-chemistry interactions. The conditions that are encountered in furnaces or gas turbine combustion chambers, where there is a recirculation of hot combustion products which contributes to flame stabilization downstream of the injection, are simulated by this burner. Therefore, the burner configuration allows investigation of stabilization mechanisms for lifted flames environments that are relevant to practical combustion applications. Two stabilization mechanisms can be suggested: auto-ignition and premixed flame propagation. In the experiments, the lift-off distance was very sensitive to small changes in the vitiated co-flow temperature. This sensitivity is a challenging modelling problem for numerical calculations.

The extensive database [1, 2, 3], thanks to use of advanced laser measurements technique, makes it a good model problem for validating calculations. In addition, it has been studied numerically within the RANS framework using PDF techniques [1, 2, 4, 5, 6], using the Eddy Dissipation Concept (EDC) [1, 7] and Conditional Moment Closure (CMC) [8]. LES of this flame has been also performed [9, 10, 11]. A range of mixing models and detailed or reduced chemical kinetics mechanisms have been applied. Good agreement between experimental and computational results has been achieved in several of the studies. All these studies indicate that the flame is largely controlled by chemical processes.

Current views on the stabilization mechanism of this flame appear to be divergent. In [2], two numerical indicators were developed to distinguish between flame stabilization by auto-ignition, as opposed to stabilization through premixed flame propagation. The indicators successfully identified auto-ignition and premixed flame propagation in simple test cases. For case [1] auto-ignition was identified as the only stabilization mechanism. However, the study of [8], using the RANS-CMC approach, reported flame stabilization by premixed flame propagation at low co-flow temperatures and by auto-ignition at high co-flow temperatures.

In the current work, a detailed reaction mechanism [12] and the LES-CMC methodology are applied. First, a qualitative description of the simulation results, by examining the instantaneous resolved temperature and species mass fraction fields, is provided. The structure of the lifted flame is further investigated by comparing the measured temperature and species mass fraction profiles and the simulation results. This will be first done for the basic case where the co-flow temperature $T_{cf} = 1045K$ is used. The sensitivity of prediction to boundary conditions is also explored. Finally, the stabilization mechanisms are addressed.

LES-CMC formulation

In LES, the filtered equations for mass, momentum and a conserved scalar, mixture fraction (ξ) are solved. Details of the LES as applied, are found in [13]. The sub-grid scale stress tensor is modeled by constant Smagorinsky model with the model constant $C_S = 0.1$ and a turbulent Schmidt number $Sc_t = 0.7$ is used. The mixture fraction variance is obtained from a gradient type model

$$\widetilde{\xi''^2} = C\Delta^2 \frac{\partial \tilde{\xi}}{\partial x_k} \frac{\partial \tilde{\xi}}{\partial x_k} \tag{1}$$

where C is constant ($C = 0.1$) and Δ is the mesh dependent filter width.

The CMC equations are solved for the conditionally filtered reactive scalars, where the conditioning is done on ξ. The CMC equations for n species of the reaction mechanism and temperature in LES context read [13, 14]:

$$\frac{\partial Q_\alpha}{\partial t} + \underbrace{\widetilde{\mathbf{u}|\eta} \frac{\partial Q_\alpha}{\partial x_i}}_{T_1} - \underbrace{\widetilde{N|\eta} \frac{\partial^2 Q_\alpha}{\partial \eta^2}}_{T_2} = \underbrace{\widetilde{W_\alpha|\eta}}_{T_3} + \underbrace{e_Y}_{T_4}, \alpha = 1, \ldots, n \tag{2}$$

$$\frac{\partial Q_T}{\partial t} + \underbrace{\widetilde{\mathbf{u}|\eta} \frac{\partial Q_T}{\partial x_i}}_{T_1} - \underbrace{\widetilde{N|\eta} \left[\left(\frac{\partial c_{p_\eta}}{\partial \eta} + \sum_{\alpha=1}^{n} c_{p\alpha_\eta} \frac{\partial Q_\alpha}{\partial \eta} \right) \frac{\partial Q_T}{\partial \eta} + \frac{\partial^2 Q_T}{\partial \eta^2} \right]}_{T_2}$$

$$= \underbrace{\frac{1}{c_{p_\eta}} \sum_{\alpha=1}^{n} h_\alpha \widetilde{W_\alpha|\eta}}_{T_3} + \underbrace{e_Y}_{T_4} \tag{3}$$

where $Q_\alpha = \widetilde{Y_\alpha|\eta}$ represents the conditionally filtered mass fraction of the α-species. The variable η is the sample space variable for mixture fraction. The first term on the left-hand side of Eq. (2) is the unsteady term. The second term (term T_1) represents the transport by convection in physical space through the conditional velocity. The last term on the left-hand side (term T_2) represents diffusion in mixture fraction space. This corresponds to the effect of the conditional scalar dissipation rate ($\widetilde{N|\eta}$). The first term on the right-hand side (term T_3) is the conditional chemical source term. The last term on the right-hand side, i.e. the sub-grid

scale conditional flux (term T_4) accounts for the conditional transport in physical space and it is modelled as:

$$e_Y = \frac{1}{\bar{\rho}\widetilde{P}(\eta)}\frac{\partial}{\partial x_i}\left[\bar{\rho}\widetilde{P}(\eta)D_t\frac{\partial Q_\alpha}{\partial x_i}\right] \text{ or } e_Y = \frac{1}{\bar{\rho}\widetilde{P}(\eta)}\frac{\partial}{\partial x_i}\left[\bar{\rho}\widetilde{P}(\eta)D_t\frac{\partial Q_T}{\partial x_i}\right] \tag{4}$$

For complete closure of Eqs. (2) and (3), models are required for $\widetilde{u|\eta}$ and $\widetilde{N|\eta}$ as well. The assumption that the conditional velocity is equal to unconditional velocity for entire mixture fraction range is made here. For the scalar dissipation rate, the Amplitude Mapping Closure (AMC) model [15] is used. This model requires an unconditional filtered scalar dissipation rate, modelled as:

$$\widetilde{N} = \left(\frac{\nu}{Sc} + \frac{\nu_t}{Sc_t}\right)\frac{\partial\widetilde{\xi}}{\partial x_k}\frac{\partial\widetilde{\xi}}{\partial x_k} \tag{5}$$

Eqs. (2) and (3) are solved on a coarser grid than the LES and hence information for conditionally filtered velocity, turbulent diffusivity and scalar dissipation is needed. The conditionally filtered velocity is found by applying volume averaging and the model for the conditional quantities. The turbulent diffusivity $(D_t = {\nu_t}/{Sc_t})$ is also calculated using the volume averaging. The conditional scalar dissipation rate is found by calculating the volume averaged unconditional scalar dissipation rate and applying the AMC model at the CMC resolution. More details are found in [13, 14].

First order closure is provided for the chemical reaction rate and it is evaluated using the conditionally filtered reacting scalars.

The unconditional and conditional filtered values are related by:

$$\widetilde{Y}_\alpha = \int_0^1 \widetilde{Y_\alpha|\eta}\,\widetilde{P}(\eta)d\eta \tag{6}$$

Test Case
The Berkeley burner [1] consists of a fuel jet nozzle and a surrounding perforated disk. The jet nozzle inner diameter is 4.57mm (*d*) and the wall thickness is 0.89mm. The outer disk has a diameter of 210mm. At the fuel nozzle exit the co-flow properties are uniform. Table 1 summarizes the boundary conditions. The stoichiometric mixture fraction is 0.474. The uncertainties in the temperature measurements are estimated to be around 30K.

Table 1. Boundary conditions [1, 4].

Item	Co-flow	Fuel jet
Velocity [m/s]	107	3.5
Temperature [K]	1045	305
$X(H_2)$ [-]	0.0005	0.2537
$X(O_2)$ [-]	0.1474	0.0021
$X(N_2)$ [-]	0.7534	0.7427
$X(H_2O)$ [-]	0.0989	0.0015

Numerical methods and model options
The computational domain extends axially 30*d* downstream from the jet inlet (137mm) and radially up to 20*d* (91.4mm). Results are obtained with grids comprising 192 x 48 x 48 cells

(LES) and 80 x 4 x 4 cells (CMC). The LES grid is stretched smoothly toward the co-flow in the radial direction and is expanded smoothly in the axial direction. The jet inlet is resolved with 12 x 12 cells in the inflow (*x-z*) plane. The CMC grid is expanded smoothly only in the axial direction. The mesh in mixture fraction space consists of 51 nodes, clustered around the most reactive mixture fraction.

Table 2. Most reactive mixture fraction.

T_{cf} [K]	1022	1030	1038	1045	1060	1080
η_{mr} [-]	0.0639	0.0639	0.0587	0.0534	0.0482	0.0482

The most reactive mixture fraction is determined with a stand-alone 0D-CMC where the micro-mixing is switched off by using a scalar dissipation rate of $10^{-20}s^{-1}$, giving thus a parallel solution for a series of homogeneous reactors of variable mixture fraction. The auto-ignition criterion based on an increase of the OH mass fraction above a threshold value (2×10^{-4}) is used. The most reactive mixture fraction as function of the co-flow temperature is given in Table 2.

The simulations are started from a developed inert flow field. After 20ms, statistics are collected over a period of 32.5ms and time averaged data are compared to the measurements. The lift-off height is defined as the location where OH mass fraction reaches 2×10^{-4} [4].
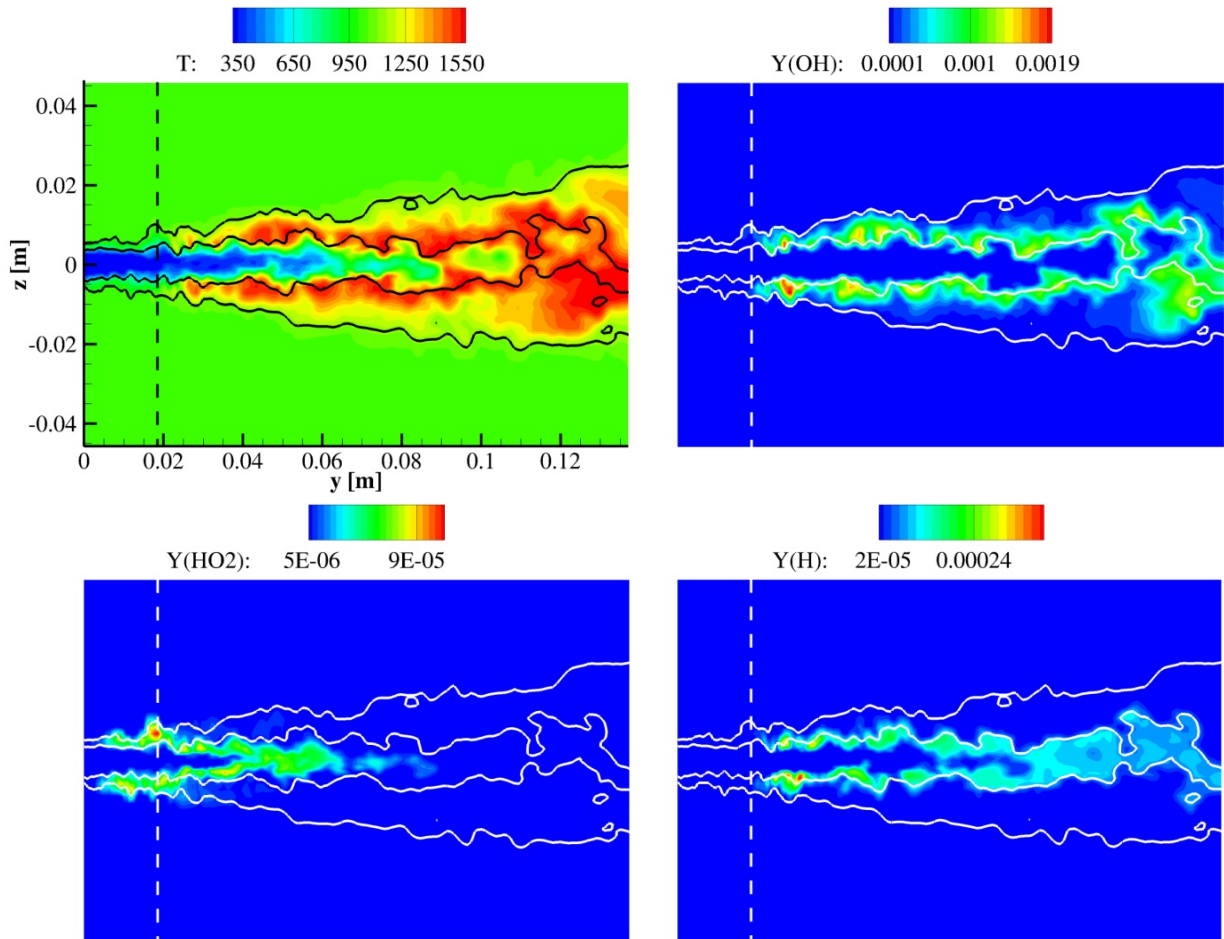
Figure 1. Instantaneous resolved temperature, OH, HO$_2$ and H mass fraction fields in a symmetry plane. Inner isoline: η_{st}, outer isoline: η_{mr}.

Results

Instantaneous temperature and species mass fraction ($Y(OH)$, $Y(H)$ and $Y(HO_2)$) fields are given in Fig. 1 at the end time of the simulations for co-flow temperature $T_{cf} = 1045K$. The lift-off height is less than ten nozzle diameters ($10d = 45.7mm$). For this temperature the lift-off height is about $4d$. The ignition length of $10d$ is obtained for a co-flow temperature of 1030K in the simulations (see below). The uncertainty in the temperature measurements was in the order of 30K [1], so that the use of $T_{cf} = 1030K$ as inlet boundary condition remains within experimental error. It is clear that HO_2 is generated long before the reaction zone, consistent with its role as an auto-ignition precursor. The highest concentration of HO_2 is found between the most reactive and stoichiometric mixture fraction upstream the flame base in the fuel-lean pre-ignition zone. Some HO_2 survives in the fuel-rich reaction zones of the flame and is depleted in the post-flame zones. Subsequently, after build-up of HO_2, generation of radicals (OH and H) occurs.
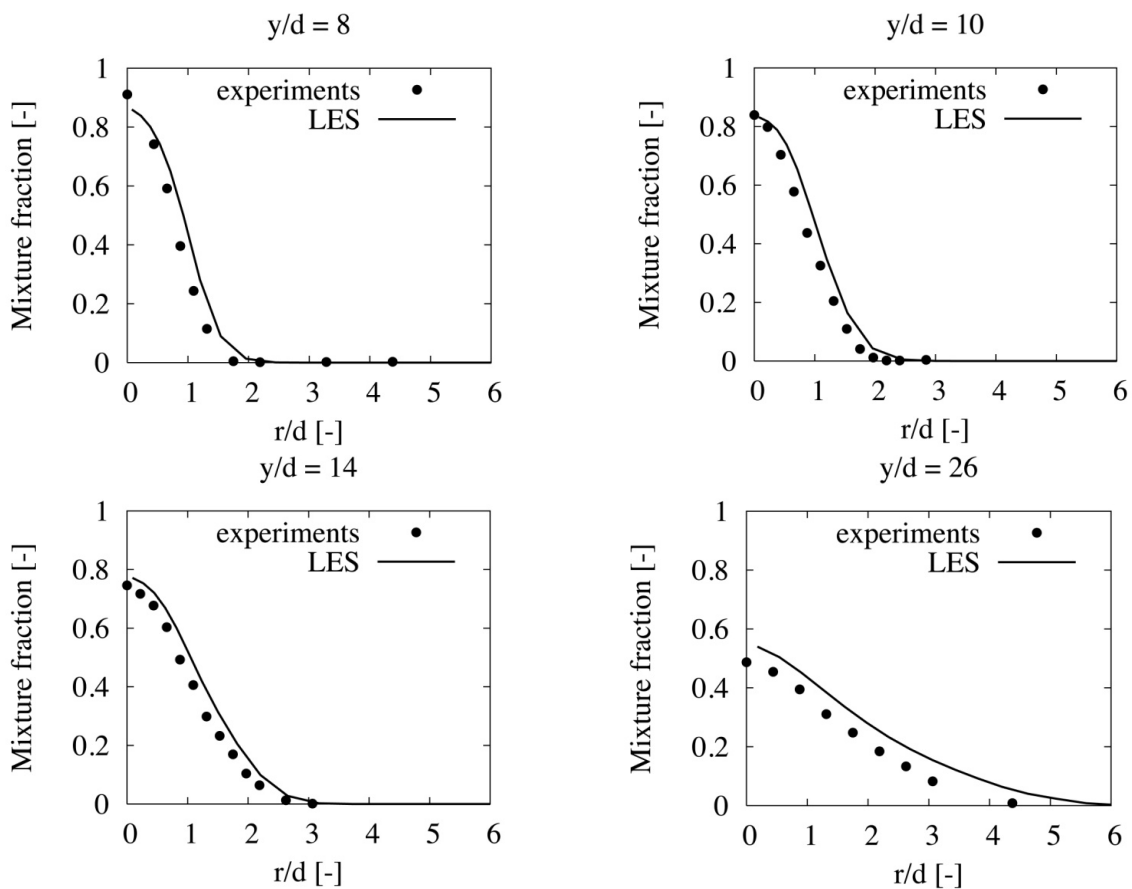
Figure 2. Radial profiles of mixture fraction at four axial stations.

The radial profiles at various axial locations ($y/d = 8, 10, 14, 26$) in the lifted flame are shown in Figs. 2 and 3 for the conditions listed in Table 1. Good agreement is observed at most axial positions. The good quality of mixture fraction profiles is very important for the quality of the values for all species. The OH radical is a good indicator of the chemistry activity. After occurrence of auto-ignition (at $y/d = 10$ in experiments), OH concentrations increase by several orders of magnitude - a trend that is well captured by the computations albeit with the shift in the ignition location. The oxygen mass fraction profiles deviate downstream, particularly in the region between $r/d < 1$, where the oxygen mass fraction is strongly under-predicted. This is caused by the early ignition (lift-off height is $4d$ while in the

experiments is 10d). Much better agreement is obtained when the co-flow temperature is decreased in order to obtain the lift-off height close to $H/d = 10$, as shown below.
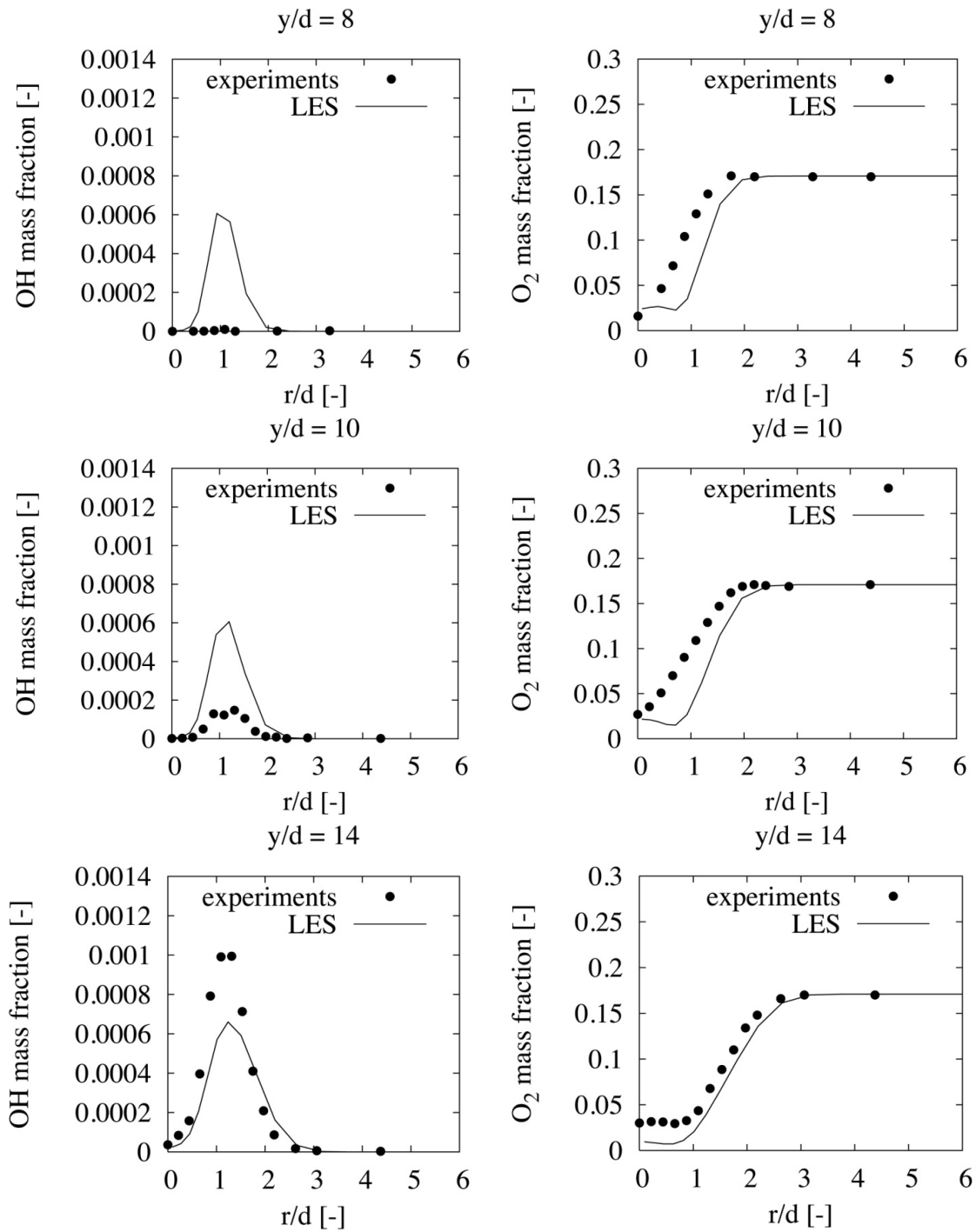
Figure 3. Radial profiles of OH and O_2 mass fractions at three axial stations.

Fig. 4 shows the lift-off heights (H) from the simulations for a range of a co-flow temperatures (T_{cf} = 1022K, 1030K, 1045K, 1060K and 1080K), compared with the data measured independently by Cabra et al. [1], Gordon et al. [2] and Wu et al. [3]. The Gordon et al. results (a) and (b) indicate measurements taken from two separate experiments. The uncertainty in the temperature measurements of Cabra et al. [1] is indicated by the horizontal line. With T_{cf} = 1080K, an attached flame is found in the simulations. When the temperature is

reduced, a lifted flame is observed. The simulation results are in good agreement with the measurements of [3]. Indeed, the high sensitivity of the lift-off height to the co-flow temperature makes it hard to obtain absolute agreement with the measurements. The discrepancy may be due to a combination of experimental measurements, different definitions of lift-off height or the chemistry mechanism used for simulations. The possible impact of the chemistry mechanism has been discussed in [16].
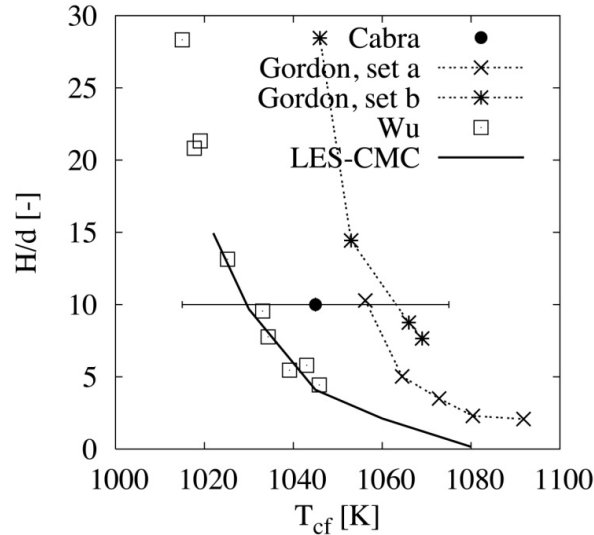

Figure 4. Lift-off height as a function of the co-flow temperature.

Fig. 4 also suggests that, in order to make sensible comparisons between calculations and measurements, flames with the same lift-off height, rather than the same co-flow temperature, should be selected for comparison with the measurements. Therefore, radial profiles at different axial locations are discussed next for $T_{cf} = 1030K$ (Fig. 5). Comparison to Fig. 3 reveals that now the position of ignition is well predicted. The profiles being slightly wide, the quantitative agreement, even for the minor species OH, is good.

The stabilization of the lifted flames can be governed by auto-ignition or premixed flame propagation. Stabilization mechanisms of the lifted flames have received a lot of attention lately due to their great importance in industry. The analysis of a time history of the radical concentrations or the convection-diffusion-reaction (CDR) budgets, i.e. the analysis of each term in the CMC transport equations, can aid in the identification of the dominant flame stabilization mechanism, as suggested in [2]. Following [2], the flame will be stabilized by auto-ignition if the HO_2 radical builds up prior the build up of H, O and OH and if CDR budgets show a convection-reaction balance. On the other hand, if the mass fractions of all the radicals begin increasing at the same point, the flame is stabilized by premixed flame propagation. In this case, a convection-diffusion balance is present at the locations upstream of the flame base, with the chemistry term relatively small. In the reaction zone, there should be a balance between diffusion and reaction.

Fig. 6 shows instantaneous resolved OH and HO_2 fields in a symmetry plane for two co-flow temperatures. For the first case, with $T_{cf} = 1030K$, it is clear that HO_2 is generated long before the flame stabilization point is reached. The HO_2 radical is present more than $10d$ below the flame base. This build-up of the HO_2 radical upstream the flame base, prior to ignition, is one of the indicators the auto-ignition stabilization. In case of $T_{cf} = 1060K$, the HO_2 radical build up occurs very close to injector nozzle, less than $2d$ upstream of the OH generation. The concentration of the HO_2 radical is also much lower than for the cases with lower co-flow temperatures. As can be seen above (Fig. 4), for higher co-flow temperatures,

the lift-off height also becomes less sensitive to the changes in the co-flow temperature. This makes it unclear if the flame is still stabilized by auto-ignition, with short ignition delay time, since the high co-flow temperature is accelerating the reactive processes.
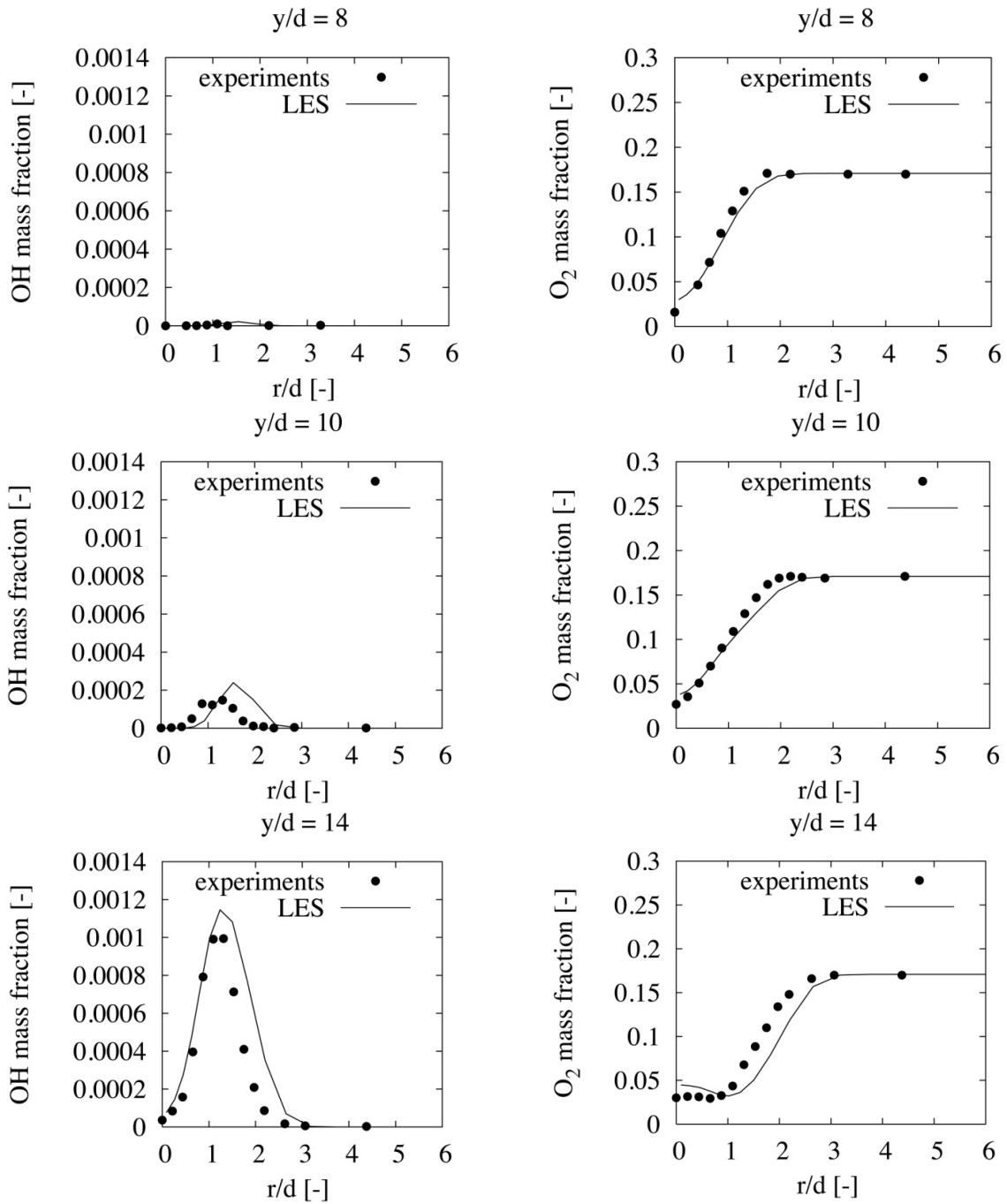

Figure 5. Radial profiles of OH and O_2 mass fraction at three axial stations.

In order to further clarify the stabilization mechanism of the flames under study, the balance of the terms in the CMC equation for the temperature (Eq. 3) is examined. The averaged contribution of each term is plotted at three different axial locations along the centerline: $y/d = 1.05, 2.3, 9.7$. The axial locations cover the pre-ignition region (upstream of the flame base), as well as the flame. The balance of the terms is discussed for two co-flow temperatures: 1030K (under these conditions the obtained lift-off height is closest to $10d$) and 1060K (the flame stabilizes near the injector). In Fig. 7 (left) results for $T_{cf} = 1030$K are

presented. In this case, the location $y/d = 9.7$ corresponds to the flame base. At the flame base, the chemical source term is a few orders of magnitude higher than at the other locations.

When the co-flow temperature is increased, no significant differences are observed in the results. In this case, the lift-off height is about $2.1d$. Upstream and at the flame base, the convection-reaction balance is obtained, with non-negligible the scalar dissipation rate term. The fact that the diffusion in physical space is negligible confirms that the flame for $T_{cf} = 1060K$ is stabilized by auto-ignition, which was not readily concluded from Figure 6.
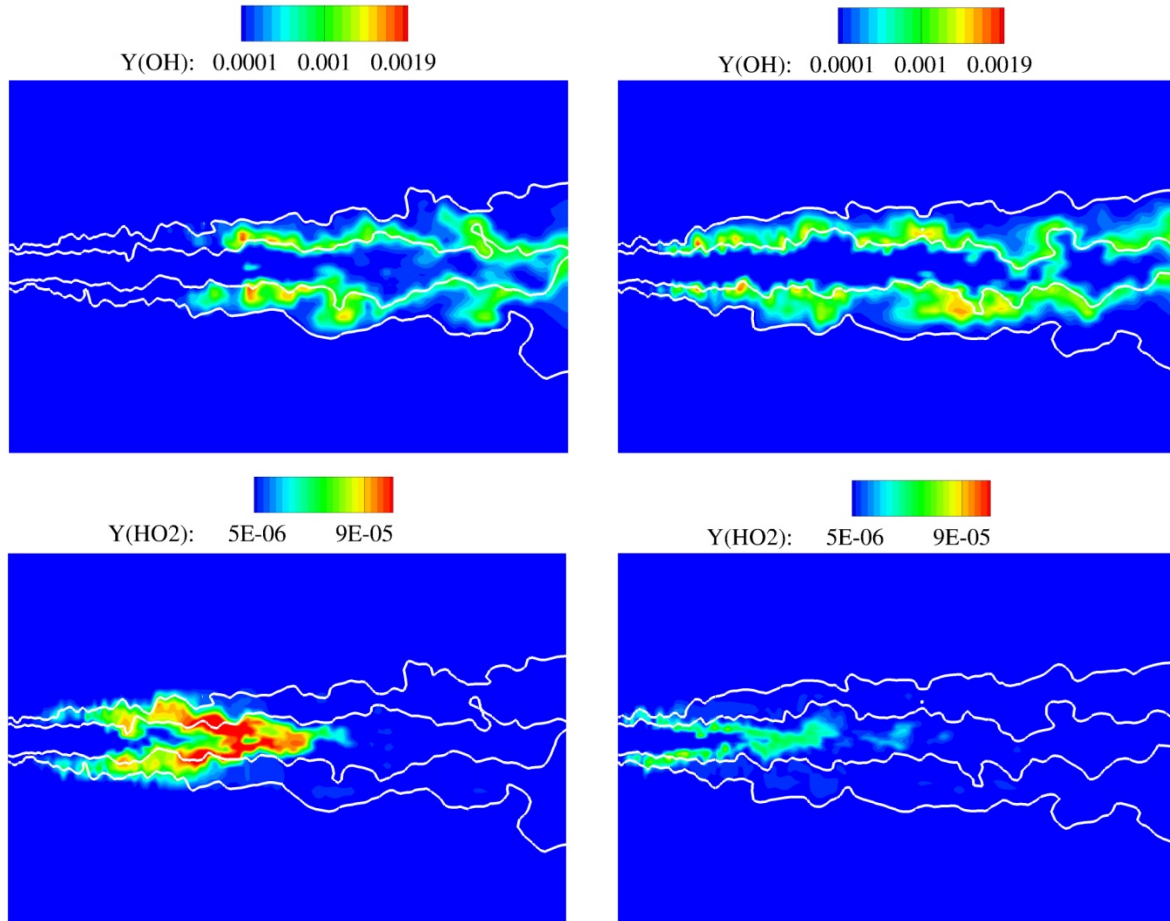
Figure 6. Instantaneous resolved OH and HO_2 mass fraction files in a symmetry plane. Left: $T_{cf} = 1030K$. Right: $T_{cf} = 1060K$.

Care must be taken in the interpretation of the results. Indeed, the observations are valid only within the modelling framework as applied. To be more precise, the effect of premixed flame propagation should be captured with the term T_4 (e_Y term in the CMC equations), i.e. diffusion in physical space, which is modelled using gradient transport model. The question arises whether this model captures the diffusion in physical space correctly. Yet, the generally good agreement with the experimental data indicates that the potential error is probably small.

Moreover, the observations are in agreement with the findings of [2] where the Berkeley case was examined applying above mentioned indicators for the determination of the stabilization mechanism. Only in the RANS-CMC calculations of [8], for the 1025K case, the lift-off height was reported to be controlled by premixed flame propagation, where strong axial diffusion and a weak chemical term were found upstream the flame base. For the 1080K case, the auto-ignition was suggested as controlling mechanism in [8].
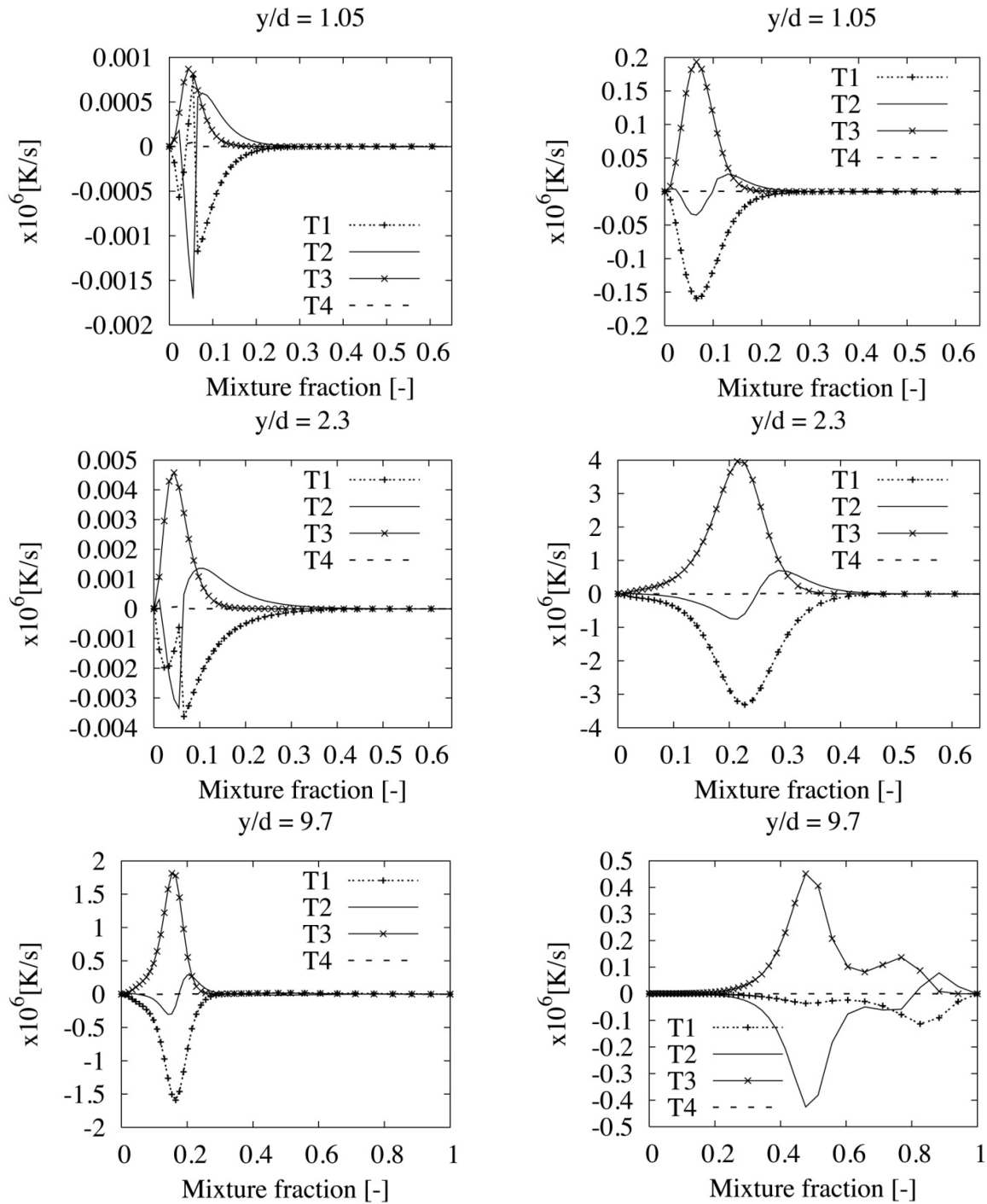
Figure 7. The terms in the CMC equation for the conditional temperature for T_{cf} = 1030K (left) and T_{cf} = 1060K (right). Note the different scale for each figure. (T_1 – convection; T_2 – sc. dissi. rate; T_3 – chem. source term; T_4 – diffusion, see Eq. 3)

Conclusions

The LES-CMC model with detailed chemistry has been applied to a lifted hydrogen flame, studied experimentally at Berkeley University. The model is able to capture the axial and radial profiles of mixture fraction, temperature and major species, such as H_2, O_2, N_2, OH and H_2O, provided the co-flow temperature is chosen appropriately. The effect of the co-flow temperature has been investigated. The lift-off height is confirmed to be very sensitive to the co-flow temperature.

A lift-off height of ten nozzle diameters was obtained experimentally for a co-flow temperature of 1045K. In the calculations, the best agreement was obtained for the co-flow temperature of 1030K, which is within experimental uncertainties. Obviously, the chemical mechanism used in the simulations will also affect the value of the lift-off height. Good agreement of species mass fraction radial profiles is obtained when the lift-off height is correct.

The stabilization mechanism, auto-ignition or premixed flame propagation, was explored by quantifying the balance of the terms in the CMC equation for temperature, as well as by examining contour plots of the species mass fractions. No evidence of premixed flame propagation is found: the diffusion in physical space is negligible for all studied conditions. Upstream of the flame base, a clear convection-reaction balance was observed, with the scalar dissipation being important as well. Inside the reactive zone, the scalar dissipation rate is dominant in balancing the chemistry, approaching the well-known structure of a non-premixed flame. HO_2 is formed well before the flame stabilization point, consistent with its role as auto-ignition precursor.

Nomenclature

C	constant in the model for mixture fraction variance
c_p	specific heat capacity at constant pressure
D	diffusivity
d	diameter
e_Y	Sub-grid scale conditional flux
H	lift-off height
h	enthalpy
N	scalar dissipation rate
P	probability density function
Q	conditional expectation of a reactive scalar
Sc	Schmidt number
t	time
T	temperature
u	velocity
W	chemical reaction term
X	species mole fraction
x	position component
Y	species mass fraction
y	axial direction
Δ	cell size
η	sample space variable for mixture fraction
v	kinematic viscosity
ρ	density
ξ	mixture fraction
ξ''^2	mixture fraction variance

Subscripts

α	species index
cf	co-flow
k	direction
mr	most reactive
st	stoichiometric
t	turbulent

Other symbols

$\tilde{\cdot}$ Favre filtered

$\bar{\cdot}$ filtered

$\cdot|\eta$ Conditioned on $\xi=\eta$

References

[1] Cabra, R., Myhrvold, T., Chen, J.Y., Dibble, R.W., Karpetis, A.N., Barlow, R.S., "Simultaneous laser Raman-Rayleigh-Lif measurements and numerical modelling results of a lifted turbulent H_2/N_2 jet flame in a vitiated co-flow", *Proc. Combust. Inst.* 29:1881-1888 (2002).

[2] Gordon, R.L., Masri, A.R., Pope, S. B., Goldin, G.M., "A numerical study of auto-ignition in turbulent lifted flames issuing into vitiated co-flow", *Combust. Theory Model.* 11:351-376 (2007).

[3] Wu, Z., Starner, S.H., Bilger, R.W., "Lift-off heights of turbulent H_2/N_2 jet flames in a vitiated co-flow", *Proc. of the 2003 Australian Symposium on Combustion and the Eighth Australian Flame Days, The Combustion Institute* (2003).

[4] Cao, R.R., Pope, S.B., Masri, A.R., "Turbulent lifted flames in a vitiated co-flow investigated using joint PDF calculations", *Combust. Flame* 142:438-453 (2005).

[5] Gkagkas, K., Lindstedt, R. P., "The impact of reduced chemistry on auto-ignition of H_2 in turbulent flows", *Combust. Theory Model.* 13:607-643 (2009).

[6] Masri, A.R., Cao, R., Pope, S.B., Goldin, G.M., "PDF calculations of turbulent lifted flames of H_2/N_2 fuel issuing into a vitiated co-flow", *Combust. Theory Model.* 8:1-22 (2004)

[7] Myhrvold, T., Ertesvag, I.S., Gran, I.R., Cabra, R., Chen, J.Y., "A numerical investigation of a lifted H_2/N_2 turbulent jet flame in a vitiated co-flow", *Combust. Sci. Technol.* 178: 1001-1030 (2009).

[8] Patwardhan, S.S., Santanu, De, Lakshmisha, K.N., Raghunandan B.N., "CMC simulations of lifted turbulent jet flames in a vitiated co-flow", *Proc. Combust. Inst.* 32:1708-1712 (2009).

[9] Duwig, C., Fuchs, L., "Large eddy simulation of a H_2/N_2 lifted flame in a vitiated co-flow", *Combust. Sci. Technol.* 180: 453-480 (2008)

[10] Jones, W.P., Navarro-Martinez, S., "Large eddy simulation of auto-ignition with a subgrid probability density function method", *Combust. Flame* 150: 170-187 (2007).

[11] Navarro-Martinez, S., Kronenburg, A., "Flame stabilization mechanisms in lifted flames", *Flow Turb. Combust.*, in press, DOI 10.1007/s10494-010-9320-1 (2011).

[12] Li, J., Zhao, Z., Kazakov, A., Dryer, F.L., "An updated comprehensive kinetic model of hydrogen combustion", *Inter. J. Chem. Kinet.* 36:566-575 (2004).

[13] Stanković, I., Triantafyllidis, A., Mastorakos, E., Lacor, C., Merci, B., "Simulation of hydrogen auto-ignition in a turbulent co-flow of heated air with LES and CMC approach", *Flow Turb. Combust.*, in press, DOI: 10.1007/s10494-010-9277-0 (2010).

[14] Triantafyllidis, A., Mastorakos, E., "Implementation issues of the conditional moment closure model in large eddy simulations". *Flow Turbul. Combust.*, 84:481–512, 2010.

[15] O'Brien, E.E., Jiang, T.L., "The conditional dissipation rate of an initially binary scalar in homogeneous turbulence", *Phys. Fluids*, 3: 3121-3123 (1991).

[16] Stanković, I., Merci, B., "Analysis of auto-ignition of heated hydrogen/air mixtures with different detailed reaction mechanisms", *Combust. Theory Model.*, in press, DOI: 10.1080/13647830.2010.542830 (2011).